Chemical Science

ROYAL SOCIETY OF CHEMISTRY

EDGE ARTICLE

View Article Online
View Journal | View Issue

Cite this: *Chem. Sci.*, 2025, **16**, 22417

All publication charges for this article have been paid for by the Royal Society of Chemistry

Received 12th June 2025
Accepted 22nd October 2025

DOI: 10.1039/d5sc04296h

rsc.li/chemical-science

Non-contact measurement of ion mobility in single halide perovskite particles

Yu-Ling Zou, [a] Ke Li,[a] Ben Niu,[a] Bangyi Yue,[b] Qiang Chen,[b] Yuxi Tian *[a] and Wei Wang *[a]

Halide perovskites, with tunable photovoltaic properties, is one of the most attractive materials in photovoltaics. The non-negligible soft lattice in perovskites induces vacancy-mediated ion migration, which is crucial to the device's efficiency and long-term stability. However, the methodologies to quantify and directly observe ion migration often require the direct contact of a metal electrode with the perovskite materials, where interfacial interactions and interior ion migration are intertwined. Here, we developed a non-contact method to evaluate the ion mobility of $MAPbBr_3$ *via* combining PL microscopy and an interpenetrating electrode device. We demonstrated the polarization and recovery dynamics of single $MAPbBr_3$ particles in an external electric field, as measured by modulation of the optical contrast during switching of the external electric field. The PL intensity was suppressed under the external electric field, which was mainly attributed to the ion migration. And, the PL spectra showed that the blue-shift of $MAPbBr_3$ originated from lattice distortions induced by field-induced ion migration. Most importantly, we obtained an intrinsic ion mobility for single $MAPbBr_3$ particles of $(2.56 \pm 0.67) \times 10^{-10}$ cm^2 V^{-1} s^{-1} under non-contact conditions.

Introduction

In the family of halide perovskites, ion migration is a widely observed solid-state electrochemical phenomenon, attributed to their intrinsic soft ionic lattice structure and hybrid electron–ion conduction properties.[1,2] The ion migration in halide perovskites is generally considered to be an important factor leading to anomalous effects in hysteresis behavior,[3] and phase segregation,[4,5] allowing for the migration of structural defects under external stimuli, such as temperature,[6,7] photoexcitation,[8] and electric fields.[9] To understand the effect of ion dynamics on the efficiency and stability of perovskite devices, various methods have been developed to assess ion migration, including current–voltage,[10,11] impedance spectroscopy,[12] and deep-level transient spectroscopy,[13] all of which have excellent time resolution. However, it is crucial for perovskite devices to detect spatiotemporal dynamic information as well. Along these lines, imaging the dynamics of moving ions would provide insight into ion migration in perovskite materials.

Recently, the introduction of various advanced microscopy techniques has significantly enhanced the ability to perform spatially resolved characterization in different materials.[14] For instance, Kelvin probe force microscopy (KPFM) enables nanoscale spatial imaging of surface potentials,[15,16] dark lock-in thermography (DLIT) technology evaluates local power dissipation,[17] and photoluminescence (PL) microscopy, combining spatial and temporal resolution, allows real-time, quantitative analysis of *in situ* ion migration processes in perovskite materials.[18,19] To record the *in situ* migration of ions under an electric field, it is necessary to design an optimal electrode structure to study the ion migration under external stimuli. Ongoing PL imaging typically requires that the perovskite materials are fabricated as a thin film and tightly fitted to the electrode device with a lateral orientation.[20] While this is a simple and common method to characterize the quality and stability of perovskite films, the deposited films normally exhibit high defect densities, and their intrinsic ion mobility could be overestimated.[21] More importantly, the contact properties of perovskites with metal electrodes are often highly defective, and the charge transfer of this heterogeneous structure receives impediments.[22] Thus, the effects of carrier transport and interface transfer are often intertwined,[20,23] making it difficult to decouple interfacial and interior contributions and obtain intrinsic mobile ion diffusion in perovskites.[24,25] Monitoring the intrinsic ion mobility with *in situ* non-contact methods in perovskites devices is hence desirable, but is yet to be demonstrated.

In this work, we demonstrated a strategy that combined PL microscopy and interpenetrating electrode devices to reveal the effect of an external electric field on the intrinsic ion mobility of

[a]*State Key Laboratory of Analytical Chemistry for Life Science, Chemistry and Biomedicine Innovation Center (ChemBIC), School of Chemistry and Chemical Engineering, Nanjing University, Nanjing, Jiangsu 210023, China. E-mail: wei.wang@nju.edu.cn; tyx@nju.edu.cn*

[b]*High-Tech Research Institute of Nanjing University, Changzhou, Jiangsu, 213164, China*

single particles in a non-contact manner for the first time. We grew $MAPbBr_3$ perovskite particles *in situ* on an interpenetrating electrode and investigated the effect of the external electric field on the polarization dynamics of $MAPbBr_3$ particles by applying an electric field of 130 kV cm^{-1}. We found that the PL intensity of $MAPbBr_3$ particles was suppressed under the external electric field, and there was a clear correlation of both particle size and electric field intensity with the polarization dynamics, which was mainly attributed to the movement of ions. The PL spectral blue-shift experimentally demonstrated that the external electric field response of $MAPbBr_3$ originated from lattice distortions introduced by the field-induced ion migration. In particular, we obtained the ion mobility of $MAPbBr_3$ about $(2.56 \pm 0.67) \times 10^{-10}$ cm^2 V^{-1} s^{-1} at the single-particle level.

Results and discussion

Optical imaging of single $MAPbBr_3$ by photoluminescence (PL) microscopy

We spin-coated the diluted $MAPbBr_3$ solutions onto the interpenetrating electrode devices, and grew $MAPbBr_3$ particles *in situ*. The ion migration behavior of $MAPbBr_3$ particles was investigated by applying a periodic external electric field between the electrodes. As one of the typical halide perovskites, $MAPbBr_3$ undergoes polarization under an electric field, which results in the ionic movement of MA cations and Br anions in specific directions.[26] In particular, with the external electric field, the vacancies/defects formed by migrating ions, acting as non-radiative recombination centers, promote non-radiative recombination,[27] and the interfacial polarization field perturbs the radiative recombination pathways of excitons.[28] These effects lead to PL spectral shifts and pronounced PL quenching. This optical response provided a direct and quantitative probe for investigating ion migration dynamics at the single-particle level.

The PL imaging system was equipped with tailored interpenetrating electrodes. The $MAPbBr_3$ particles were uniformly dispersed on the substrate, where the studied particles were situated on the bare quartz substrate in the middle of the electrodes, without direct contact with the electrodes.[29] When an external electric field was applied between the electrodes, it induced perovskite particle polarization and drove ion migration without any current flowing through the perovskite materials. This approach effectively avoided the effects of carrier injection and interfacial charge transport layers, which facilitate the decoupling of interfacial and intrinsic contributions to reveal intrinsic mobility in perovskite materials (Fig. 1a). During the application of the external electric field, we utilized a function generator to modulate the electric field and a voltage amplifier to amplify the field. We simultaneously recorded the voltage signal from the function generator and the transistor–transistor logic signal from the camera *via* a data acquisition card. In order to have enough time to capture the migration of the ions, a square wave voltage was applied to the electrodes for a period of 30 seconds. More details about the PL imaging system and the parameters of interpenetrating electrodes are provided in Fig. S1 and S2.

$MAPbBr_3$ particle response to the external electric field

To investigate the response behavior of $MAPbBr_3$ particles under an external electric field, we performed PL imaging of individual particles. When a voltage of 130 V was applied to two electrodes separated by 10 μm, an external electric field of up to 130 kV cm^{-1} was established instantaneously in the gap. As shown in Fig. 1b, the PL switching behavior of single $MAPbBr_3$ particles on a bare quartz substrate was directly observed by applying a square-wave electric field modulation. When the external electric field was established, the PL of the $MAPbBr_3$ particle was suppressed on a time scale of 5 s and maintained a stable PL intensity thereafter. When the external electric field was removed, their PL was recovered on a similar time scale. Periodic modulation of the external electric field resulted in alternating $MAPbBr_3$ particle polarization and recovery, with periodic fluctuations being exhibited in the PL intensity trajectory of individual $MAPbBr_3$ particles (Fig. 1b). These results suggest a reversible polarization process of perovskite materials, which is consistent with previous studies.[30]

To quantitatively describe the PL switching performance, we defined the switching efficiency (SE) as the relative PL intensity difference between ON and OFF states:

$$SE = \frac{PL_{on} - PL_{off}}{PL_{on}}$$

where PL_{on} and PL_{off} are the stabilized PL intensity of the ON and OFF state, respectively (Fig. 1c). Previous studies showed that the PL intensity of perovskite films was suppressed under an external electric field. This phenomenon was mostly attributed to electric field induced ion migration processes, manifested as the formation of vacancies/defects and the generation of interfacial polarization. These effects modified the PL emission process under the external electric fields: the vacancies/defects formed by migrating ions acted as non-radiative recombination centers, promoting non-radiative recombination;[27] meanwhile, the interfacial polarization electric field perturbed the radiative recombination pathways of excitons.[28] Thus, they collectively lead to the suppression of PL emission under the external electric fields (Fig. S3). We specifically discuss them in the results below.

The correlation between the SE and the external electric field is shown in Fig. 1d and e. The PL intensity was gradually suppressed with the increase of the external electric field, indicating that a higher external electric field provided more energy to induce perovskites to undergo polarization and their ions to migrate. When more ions were involved in the migration, the displacement of the optical centroid of individual $MAPbBr_3$ increased, and a higher PL intensity contrast between ON and OFF states was obtained (Fig. S4–S6). Moreover, we applied an external electric field from zero stepwise to the maximal field (90–130 kV cm^{-1}) to verify the reversible behavior (Fig. S7). It is worth mentioning that electron–hole charge separation is not negligible under the electric field, and this process usually suppresses the radiative recombination pathway, leading to the reduction of PL intensity.[31] As the nanosecond decay and second decay were attributed to electron dynamics and ion

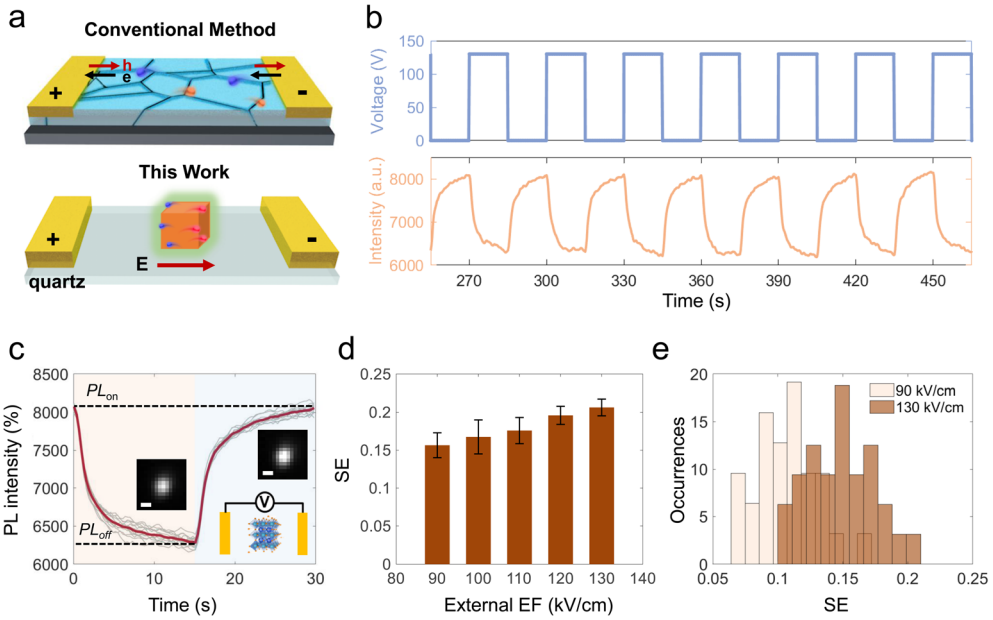

Fig. 1 The optical measurements of $MAPbBr_3$ under an external electric field. (a) The schematic of a classical contact perovskite device (top) and the electric field-induced non-contact perovskite device in this work (bottom). (b) The evolution of PL intensity with time under external electric field control. (c) The evolution of the PL intensity for a 10-cycle superposition (grey line) and the average curve (red line). The inset is the raw image of individual $MAPbBr_3$ particles with/without the external electric field. (d) The switching efficiency of an individual particle with different external electric fields in 10 cycles. (e) The histogram of switching efficiency for 43 particles at different external electric fields.

dynamics, respectively; ion migration was the dominant process for PL switching of $MAPbBr_3$ particles in the presence of an external electric field.[32,33] This slow-decaying PL image facilitated us to analyze the ion dynamics under an external electric field, and achieved the intrinsic ion mobility measurement of perovskite particles.

Ion mobility of single $MAPbBr_3$ particles

To understand the intrinsic ion mobility of $MAPbBr_3$ particles, we recorded the PL intensity evolution of $MAPbBr_3$ particles with different sizes at room temperature and carried out dynamics analyses under electric field switching processing (Fig. S8). To compare the polarization dynamics for particles of different sizes, we standardized the PL intensity of the $MAPbBr_3$ particles by the corresponding initial intensity, and superimposed the evolution of the PL intensities for each cycle. Representative PL optical curves of three individuals with different side lengths (658 nm, 871 nm, and 1270 nm) were further analysed in detail as shown in Fig. 2a–f. The blue area represented the case after the withdrawal of the electric field, while the orange area represented the case with a 130 kV cm^{-1} electric field. Considering that the single particle possesses PL blinking behavior, this leads to fluctuations in its PL intensity. Thus, we counted and averaged the polarization and recovery dynamics over 10 cycles of PL curves to mitigate the effect of fluctuations on the quantitative analysis. Considering that the perovskite particles were almost certainly not experiencing a temporally constant electric field. Specifically, the initial decay process correlated with rapid ion migration driven by a strong internal electric field. Subsequently, charge redistribution caused by ion migration induced a screening effect, leading to a gradual weakening of the internal electric field. This process manifested as slower decay dynamics. To accurately describe this time-dependent internal electric field evolution and its impact on PL dynamics, we fit the PL decay curves of perovskite materials *via* a biexponential function, which can be well fitted with the experimental data:

$$\Delta I(t) = I_0 + I_1\, e^{-\frac{t}{\tau_1}} + I_2\, e^{-\frac{t}{\tau_2}}$$

$$\tau = \frac{I_1\tau_1 + I_2\tau_2}{I_1 + I_2}$$

where I_0 is the optional constant offset component, τ_1 and τ_2 are the time constants, I_1 and I_2 are the related pre-exponential factors, and τ is the average PL dynamic time. Before the electric field switching (0–5 s), the PL intensities of all particles were stable, indicating that the recovery (polarization) process had been completed. Subsequently, the electric field was switched (5–20 s) and the $MAPbBr_3$ particles began to polarize (recovery). Obviously, dynamics times with polarization and recovery processes were significantly faster for the smaller particles (#1, Fig. 2a and b) than for the larger ones (#3, Fig. 2c and f). The electron dynamics was typically at the nanosecond time scale when exciton radiative and non-radiative recombination was the main decay process.[34] Considering that all dynamics in our work were slow processes, the polarization and recovery time of all $MAPbBr_3$ particles were on the second scale, which was consistent with the assumption that the inner ions of the $MAPbBr_3$ particles migrate under an external electric field.

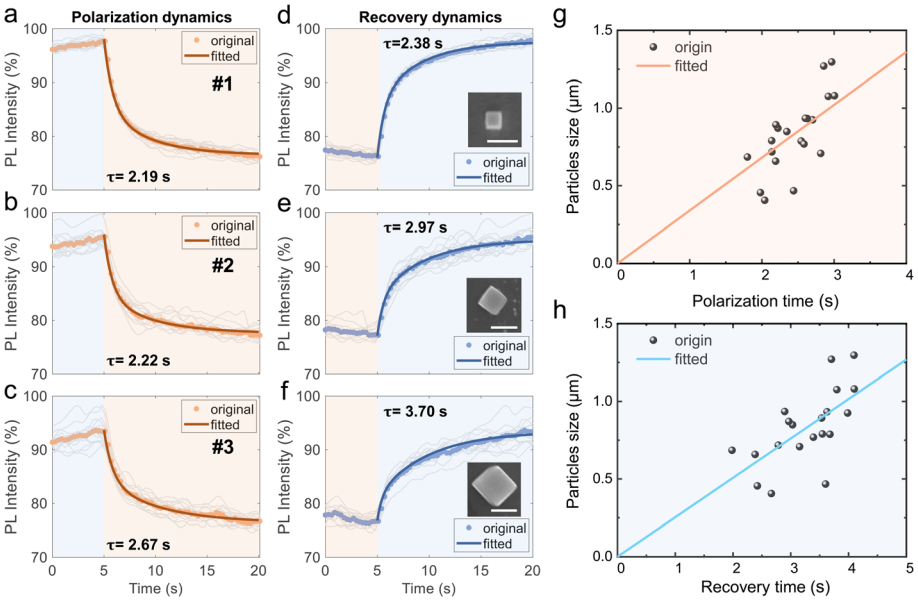

Fig. 2 The polarization and recovery dynamics with different sizes. The polarization process and recovery process of three individuals with side lengths of (a and d) 658 nm, (b and e) 871 nm, and (c and f) 1270 nm at 130 kV cm^{-1}. The scale bar is 1 μm. (g and h) Linear correlation of the dynamic time constant with particle size.

To further validate the size-dependent electric field polarization dynamics of $MAPbBr_3$, we analyzed the optical response curves of 20 $MAPbBr_3$ individuals in the field of view. The corresponding polarization and recovery time of individuals are plotted in Fig. 2g and h, respectively. Although the particle heterogeneity resulting from the synthesis process caused data dispersion, the polarization (recovery) time generally still showed a gradual increase with increasing particle size. Previous studies showed that the ion drift velocity can be expressed as $v = L/\tau$, where L is the channel length.[1] Considering that the single halide perovskite particles were non-contact with the electrodes in our work, it is reasonable that their channel length was expressed as the size of particles, and size linearly correlated with the polarization (recovery) time. Moreover, since the ion drift velocity is a function of both the intrinsic material properties and the external driving force, we will further discuss the influence of external electric fields on ion migration in the following discussion.

To understand the external electric field dependence of ion mobility, we counted and analysed the dynamic evolution of the $MAPbBr_3$ particles under different external electric field strengths from 90 to 130 kV cm^{-1} for 10 cycles each. All the measured optical curves of $MAPbBr_3$ particles were statistically taken into account to get the average curves and polarization (recovery) time (Fig. 3a, b and S9). The polarization and recovery times of 43 particles were collected to construct histograms (Fig. 3c). As the electric field increased, we found that the polarization dynamics were related to the external electric field switching magnitude, while the recovery dynamics were uncorrelated with that. For the former (polarization), this was attributed to that, at a larger external electric field, the alignment of the ion was easier, requiring less polarization time and faster dynamics.[35,36] For the latter (recovery), the external electric field was switched to zero, in other words, the external electric field was uninvolved in the recovery process and did not interfere with its dynamics. Then, we described the velocity of the ion migration as a function of the external electric field. By applying the various external electric fields, we found that the polarization dynamics were proportional to the external electric field, as shown in Fig. 3d. This ion migration can be described by a simple theory, which was based on a first-order approximation that neglected ion diffusion:[37,38]

$$\mu_{ion} = \frac{v}{E}$$

where the μ_{ion} is defined as the ratio between the ion drifting velocity (v) and external electrical field strength. We plotted drifting velocity *versus* the external electric field, and found that both are essentially linearly correlated (Fig. S10), suggesting that the formula was applicable. Moreover, we performed statistics on the calculated ion mobility and plotted the corresponding histograms (Fig. 3e). By fitting the field-dependent ion migration, the mobility of ions can be obtained as $(2.56 \pm 0.67) \times 10^{-10}$ cm^2 V^{-1} s^{-1}. Following the Einstein relation,[39] the correlation between ion mobility and diffusion coefficient (D) is established as:

$$D = \mu_{ion} k_B T / q$$

where k_B is the Boltzmann constant, T is the absolute temperature, and q is the electron charge. Thus, we obtained a diffusion coefficient of around 6.58×10^{-12} cm^2 s^{-1} for single $MAPbBr_3$ particles, which was consistent with that of single crystals.[40]

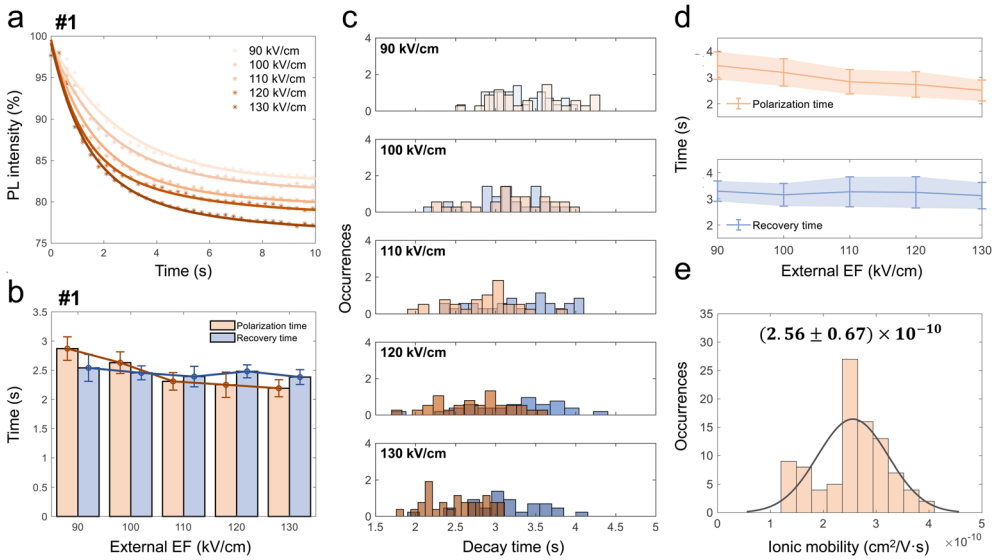

Fig. 3 The ion mobility of single $MAPbBr_3$ particles under different external electric fields. (a) The PL curves of the polarization process under different external electric fields of the representative individual $MAPbBr_3$ particle. The solid lines are the corresponding fitting results. (b) The evolution of polarization and recovery time to external electric fields of the representative individual $MAPbBr_3$ particle. (c) The histogram of the polarization (orange) and recovery (blue) time under different external electric fields. (d) The evolution of the statistical polarization and recovery time to the external electric field. (e) The histogram of ion mobility.

Electrically driven reversible blue-shifted PL of $MAPbBr_3$ particles

To verify the influence of the electric field on ion migration, we tracked the PL emission spectra of individual $MAPbBr_3$ particles in the presence of an external electric field. Before performing the PL spectra measurements, we calibrated the combination of the spectrograph and the camera, and corresponded each pixel of the spectral images to the wavelength (Fig. S11). The single $MAPbBr_3$ particle was exposed to a periodic applied electric field and excited at 445 nm, while the PL spectra of single particles were recorded (Fig. 4a). The PL spectra absence/presence of 130 kV cm^{-1} electric field modulation was indicated at the bottom (blue/orange block). It was found that the PL intensity decayed in the presence of an external electric field, which was consistent with the above results.

To clarify the modulation of the PL spectra, we carried out the Lorentzian-fitting to the spectra of each frame and obtained the PL peak positions.[41] Fig. 4b presents blue regions showing the PL spectral shift between subsequent frames without an external electric field, where the PL shift of the mean frame was around 0 nm (blue). In contrast, the spectral shift between subsequent frames with an external electric field modulated at 130 kV cm^{-1} (orange) exhibited an average frame shift of −0.86 nm towards higher energy emission. Previous studies showed that in the presence of the electric field, ion migration from the polarization of perovskite particles can cause lattice distortions, which modulated their energy bandgap and resulted in spectral blue-shift.[4] Once the external electric field was removed, the ions were driven by the mixing entropy and the concentration gradient to fill the original position. The $MAPbBr_3$ particles exhibited reversible blue-shift of the PL spectra under a periodic external electric field, which was attributed to the migration of the ions and subsequent lattice distortion.

To further understand the electrically driven reversible blue-shifted PL of $MAPbBr_3$ particles, we monitored the evolution of the PL shift at different external electric fields (Fig. S12). Obviously, the PL peak position exhibited a reversible spectral blue-

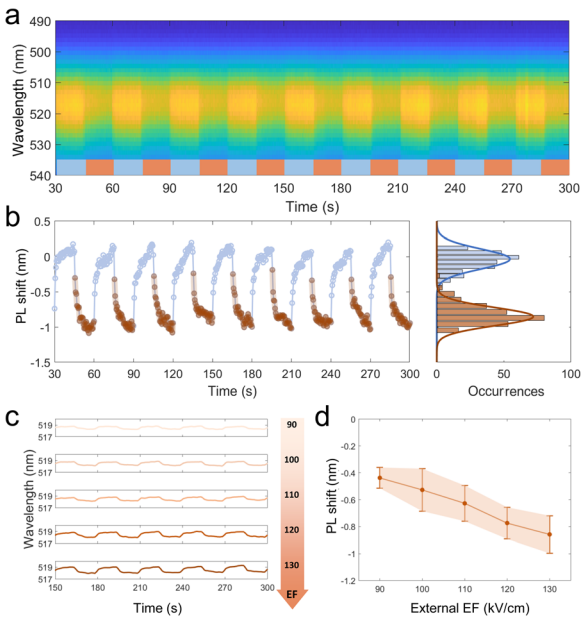

Fig. 4 The PL spectra of $MAPbBr_3$ single particle with the modulation of the external electric field. (a) The pseudo-colored successive spectra of the representative single $MAPbBr_3$ particle without/with external electric field for the 0 V to 130 kV cm^{-1} measurement. (b) The PL shift between subsequent frames 'without external electric field' and 'with external electric field' from the measurement. The left panel was the time trace of PL shift. The right panel was the histogram of PL shifts fitted by a normal distribution. (c) The Lorentzian-fitted PL peak position of successive spectra under the different external electric fields. (d) The evolution of PL spectral shifts with external electric fields.

shift during electric field cycling of individual particles, and the blue-shift increased when applying a larger external electric field (Fig. 4c). We performed histogram statistics for the spectral shift in the absence/presence of the external electric field, and they possessed normally distributed probabilities induced by the spectral shift (Fig. S13). From this, we extracted the most probable PL peaks, and associated them with the external electric field, as shown in Fig. 4d and S14. The field-induced spectral shifts were found to be linear, namely, shifting to higher energies due to an increase in the external electric field. The linear correlation of the spectral blue-shift with the external electric field was consistent with the above trend of field-induced dynamics evolution (Fig. 3d). The migration of ions was facilitated by the higher external electric field, which further shortened the polarization time and modified the Pb–Br bond angle and length, leading to subsequent lattice distortion and increased blue-shift.

Conclusions

In summary, we developed a strategy combining PL microscopy and an interpenetrating electrode device to monitor the polarization and recovery processes of single perovskite particles in a quantitative, non-contact, and high-throughput manner. With this strategy, direct contact between the metal electrode and the perovskite material was avoided. It not only achieves the decoupling of interfacial and interior contributions, but also facilitates the investigations on single nanoparticles, where microfabrication of metal–perovskite–metal configurations can be technically challenging. The PL intensity of $MAPbBr_3$ particles was suppressed under an external electric field, which was dominated by the migration of the ions and their triggered chemical processes. The size-dependent and field-dependent polarization dynamics of $MAPbBr_3$ were further investigated at the single particle level, and both showed significant correlations with the dynamics time. In addition, the PL spectra were investigated for the energy shift of $MAPbBr_3$ under the external electric field, which was suggested to originate from lattice distortions caused by field-induced ion migration. Combining PL images and spectra, the ion mobility of $MAPbBr_3$ was deduced to be around $(2.56 \pm 0.67) \times 10^{-10}$ cm^2 V^{-1} s^{-1} at the single-particle level. It offers the potential for non-contact evaluation of novel optoelectronic materials.

Author contributions

W. W. conceived the idea, and W. W. and Y. T. supervised this project. Y.-L. Z., B. N., B. Y., and Q. C. carried out the photoluminescence experiments. K. L. synthesized the $MAPbBr_3$ particles. W. W. and Y.-L. Z. analysed the data and wrote the manuscript. All authors contributed to reviewing and editing the final manuscript. Collaboration of this work was managed by W. W. and Y. T.

Conflicts of interest

There are no conflicts to declare.

Data availability

The data supporting this article have been included as part of the supplementary information (SI). Supplementary information: details of experimental methods, characterisation data. See DOI: https://doi.org/10.1039/d5sc04296h.

Acknowledgements

This work was supported by the National Natural Science Foundation of China (No. 21925403 and 22073046), the Excellent Research Program of Nanjing University (Grant No. ZYJH004), and the Science and Technology Support Program (Industry Foresight and Key Core Technologies) of Changzhou (CE20230011).

Notes and references

1 N. Yantara and N. Mathews, *Joule*, 2024, **8**, 1239.
2 V. Hazra, A. Mandal and S. Bhattacharyya, *Chem. Sci.*, 2024, **15**, 7374.
3 Q. Xiong, C. Wang, Q. Zhou, L. Wang, X. Wang, L. Yang, J. Ding, C.-c. Chen, J. Wu, X. Li and P. Gao, *Adv. Funct. Mater.*, 2022, **32**, 2107823.
4 H. Zhang, X. Fu, Y. Tang, H. Wang, C. Zhang, W. W. Yu, X. Wang, Y. Zhang and M. Xiao, *Nat. Commun.*, 2019, **10**, 1088.
5 M. Lee, J. A. Vigil, Z. Jiang and H. I. Karunadasa, *Chem. Sci.*, 2025, **16**, 9662.
6 J. Cao, S. X. Tao, P. A. Bobbert, C.-P. Wong and N. Zhao, *Adv. Mater.*, 2018, **30**, 1707350.
7 X. Xiao, J. Dai, Y. Fang, J. Zhao, X. Zheng, S. Tang, P. N. Rudd, X. C. Zeng and J. Huang, *ACS Energy Lett.*, 2018, **3**, 684.
8 Y.-T. Li, L. Ding, J.-Z. Li, J. Kang, D.-H. Li, L. Ren, Z.-Y. Ju, M.-X. Sun, J.-Q. Ma, Y. Tian, G.-Y. Gou, D. Xie, H. Tian, Y. Yang, L.-W. Wang, L.-M. Peng and T.-L. Ren, *ACS Cent. Sci.*, 2019, **5**, 1857.
9 T. Roh, H. Zhu, W. Yang, A. Liu and Y.-Y. Noh, *ACS Energy Lett.*, 2023, **8**, 957.
10 J. Zhang, X. Niu, C. Peng, H. Jiang, L. Yu, H. Zhou and Z. Zhou, *Angew. Chem., Int. Ed.*, 2023, **62**, e202314106.
11 X. Ji, Y. Zhao, X. Chen, S. Zhang, L. Zhan, H. Zhang, W. Zheng, W.-H. Zhu and Y. Wu, *Chem. Sci.*, 2025, **16**, 8569.
12 C. A. Aranda, A. O. Alvarez, V. S. Chivrony, C. Das, M. Rai and M. Saliba, *Joule*, 2024, **8**, 241.
13 J. Liu, M. Wang, J. Lin, G. Chen, B. Liu, J. Huang, M. Zhang, G. Liang, L. Lu, P. Xu, B. Tian, H.-S. Kwok and G. Li, *J. Mater. Chem. A*, 2022, **10**, 17237.
14 M. C. Schubert, L. E. Mundt, D. Walter, A. Fell and S. W. Glunz, *Adv. Energy Mater.*, 2020, **10**, 1904001.
15 V. W. Bergmann, S. A. L. Weber, F. Javier Ramos, M. K. Nazeeruddin, M. Grätzel, D. Li, A. L. Domanski, I. Lieberwirth, S. Ahmad and R. Berger, *Nat. Commun.*, 2014, **5**, 5001.
16 Y. Yuan, J. Chae, Y. Shao, Q. Wang, Z. Xiao, A. Centrone and J. Huang, *Adv. Energy Mater.*, 2015, **5**, 1500615.

17 O. Breitenstein, F. Fertig and J. Bauer, *Sol. Energy Mater. Sol. Cells*, 2015, **143**, 406.
18 J. Zhang, C. Li, M. Chen and K. Huang, *J. Phys. D: Appl. Phys.*, 2020, **54**, 044002.
19 D. A. Jacobs, C. M. Wolff, X.-Y. Chin, K. Artuk, C. Ballif and Q. Jeangros, *Energy Environ. Sci.*, 2022, **15**, 5324.
20 M. Saqib, Y. Fan, R. Hao and B. Zhang, *Nano Energy*, 2021, **90**, 106539.
21 Z. Le, A. Liu, Y. Reo, S. Bai, Y.-Y. Noh and H. Zhu, *ACS Energy Lett.*, 2024, **9**, 1639.
22 F. H. Isikgor, S. Zhumagali, L. V. T. Merino, M. De Bastiani, I. McCulloch and S. De Wolf, *Nat. Rev. Mater.*, 2023, **8**, 89.
23 Y. Fu, B. Xie, M. Liu, S. Hou, Q. Zhu, A. Kuhn, L. Zhang, W. Yang and N. Sojic, *Chem. Sci.*, 2024, **15**, 19907.
24 L. Chen, H. Wang, W. Zhang, F. Li, Z. Wang, X. Wang, Y. Shao and J. Shao, *ACS Appl. Mater. Interfaces*, 2022, **14**, 10917.
25 L. Gong, J. Yang, W. Sheng, Y. Zhong, Y. Su, L. Tan and Y. Chen, *CCS Chem.*, 2022, **5**, 1202.
26 L. McGovern, M. H. Futscher, L. A. Muscarella and B. Ehrler, *J. Phys. Chem. Lett.*, 2020, **11**, 7127.
27 C. Li, A. Guerrero, S. Huettner and J. Bisquert, *Nat. Commun.*, 2018, **9**, 5113.
28 Y. Su, H. Xie, C. Li, Z. Xia, W. Xu, Z. Mao, G. Zhan, K. Liao, J. Li, J. Li, J. Zhang, Y. Yin and L. Wang, *Adv. Funct. Mater.*, 2025, 2505380, DOI: **10.1002/adfm.202505380**.
29 K. Missaoui, G. Wantz, T. Toupance, S. Chambon and A. Kuhn, *Chem. Sci.*, 2025, **16**, 10691–10700, DOI: **10.1039/D5SC00802F**.
30 H. Wang, Y. Yin, J. Xu, J. Li, Y. Bao, M. An, L. Tang, S. Jin, W. Tian and Y. Yang, *ACS Nano*, 2023, **17**, 23671.
31 S. Shrestha, X. Li, H. Tsai, C.-H. Hou, H.-H. Huang, D. Ghosh, J.-J. Shyue, L. Wang, S. Tretiak, X. Ma and W. Nie, *Chem*, 2022, **8**, 1107.
32 Y. Zhao, W. Zhou, W. Ma, S. Meng, H. Li, J. Wei, R. Fu, K. Liu, D. Yu and Q. Zhao, *ACS Energy Lett.*, 2016, **1**, 266.
33 S. Zhao, J. Leng, S. Wang, X. Yan, Z. Yin, Y. Yin, J. Zhang and S. Jin, *Chem. Sci.*, 2022, **13**, 8334.
34 K. Wu, G. Liang, Q. Shang, Y. Ren, D. Kong and T. Lian, *J. Am. Chem. Soc.*, 2015, **137**, 12792.
35 R. Chen, G. Zhang, Y. Gao, L. Xiao and S. Jia, *Appl. Phys. Lett.*, 2012, **100**, 203118.
36 S. Tiewcharoen, C. Warakulwit, V. Lapeyre, P. Garrigue, L. Fourier, C. Elissalde, S. Buffière, P. Legros, M. Gayot, J. Limtrakul and A. Kuhn, *Angew. Chem., Int. Ed.*, 2017, **56**, 11431.
37 C. Li, A. Guerrero, Y. Zhong, A. Gräser, C. A. M. Luna, J. Köhler, J. Bisquert, R. Hildner and S. Huettner, *Small*, 2017, **13**, 1701711.
38 P. Fassl, S. Ternes, V. Lami, Y. Zakharko, D. Heimfarth, P. E. Hopkinson, F. Paulus, A. D. Taylor, J. Zaumseil and Y. Vaynzof, *ACS Appl. Mater. Interfaces*, 2019, **11**, 2490.
39 J. Y. Park, Y. H. Lee, M. A. Zaman Mamun, M. M. Fahimul Islam, S. Zhang, K. Ma, A. U. Gaitonde, K. Wang, S. J. Yang, A. Marconnet, J. Mei, M. A. Alam and L. Dou, *Matter*, 2024, **7**, 1817.
40 J. Xing, Q. Wang, Q. Dong, Y. Yuan, Y. Fang and J. Huang, *Phys. Chem. Chem. Phys.*, 2016, **18**, 30484.
41 S. Liu, A. S. Arce, S. Nilsson, D. Albinsson, L. Hellberg, S. Alekseeva and C. Langhammer, *ACS Nano*, 2019, **13**, 6090.